Linear and nonlinear low-frequency electrodynamics of surface superconducting states in an yttrium hexaboride single crystal

M. I. Tsindlekht, V. M. Genkin, G. I. Leviev, I. Felner, O. Yuli, I. Asulin, and O. Millo
The Racah Institute of Physics, The Hebrew University of Jerusalem, 91904 Jerusalem, Israel

M. A. Belogolovskii
Donetsk Physical and Technical Institute, National Academy of Sciences of Ukraine, 83114 Donetsk, Ukraine

N. Yu. Shitsevalova
Institute for Problems of Materials Science, National Academy of Sciences of Ukraine, 03680 Kiev, Ukraine
(Received 15 July 2007; revised manuscript received 10 April 2008; published 29 July 2008)

We report on the low-frequency dynamics of surface superconducting states in yttrium hexaboride single crystal. Tunneling and dc magnetization experiments demonstrate that YB_6 is a classical type-II BCS superconductor with a slightly suppressed order parameter near the surface. The ac response at frequencies 10–1500 Hz has been measured for fields H_0 parallel to the crystal surface. We found that for $H_0 > H_{c2}$ the dc magnetic moment completely disappeared, while the ac response exhibited the presence of surface superconductivity. Increasing H_0 above H_{c2} revealed the loss maximum in a field between H_{c2} and H_{c3} with a magnitude considerably larger than in mixed or normal states. In some dc fields the frequency dependence of the real part of the susceptibility is reminiscent of a spin-glass system. At the same time the imaginary component exhibits frequency dispersion which is not a typical feature of the classical spin-glass response. Analysis of the experimental data with the Kramers–Kronig relations showed the possible existence of the loss peak at very low frequencies. It was found that the amplitude of the third harmonic was not a cubic function of the ac amplitude (as it follows from the perturbation theory) even at very low excitation levels. It was shown that the critical state model cannot adequately describe the existing experimental data. The proposed model of a slow relaxing of the order parameter allows one to understand the origin of partial shielding and losses for $H_0 > H_{c2}$.

DOI: 10.1103/PhysRevB.78.024522 PACS number(s): 74.25.Nf, 74.25.Op, 74.70.Ad

I. INTRODUCTION

Nucleation of a superconducting phase in a thin surface sheath parallel to the sample surface dc magnetic field was predicted in 1963 by Saint-James and de Gennes.[1] They showed that the superconducting phase transition occurs in a magnetic field $H_0 \leq H_{c3} = 2.39\ \kappa H_c$, where H_c is the thermodynamic critical field and κ is the Ginzburg¡Landau (GL) parameter. Experimental confirmation of this theoretical prediction was done in numbers of publications.[2–6] Surface superconductivity of the mesoscopic samples was studied recently in Refs. 7 and 8. Zharkov *et al.*[9] in number of recent publications considered theoretically on the basis of the GL model superconducting states in finite dimensions from mesoscopic to macroscopic sizes. Surface superconducting states (SSSs) in macroscopic samples in these and other studies were treated as a giant vortex state.[9,10] Initially this approach was introduced long ago by Fink and Presson.[11]

A idea of the percolation phase transition in magnetic fields near H_{c3} was proposed recently in Ref. 12. Their experiment demonstrated the peculiarities of the ac response at $H_0 = 0.81 H_{c3}$ in Nb samples. They assumed that the superconducting transition in a decreasing magnetic field did not occur simultaneously at whole surface of the sample at H_{c3} but took place only in several surface spots and the percolation transition at which the whole surface becomes superconducting occurred only at $H_0 = 0.81 H_{c3}$.

Measurements of the low-frequency ac susceptibility, χ_1' and χ_1'', as a function of dc magnetic field, H_0, revealed the existence of a loss peak for H_0 between H_{c2} and H_{c3}.[2,3,5] The position of this peak with respect to the dc field depends on the excitation amplitude and frequency.[5] The peak intensity exceeds the observed losses in both the normal ($H_0 > H_{c3}$) and mixed ($H_0 < H_{c2}$) states. In spite of the extensive studies, the origin of the low-frequency losses in SSS is not yet clear. The first explanation of the experimental results was done on the basis of the critical state model. This model for superconductors in the SSS was developed by Fink and Barnes.[13] dc critical current measurements confirmed some conclusions of the critical state model.[6] For an ac response the critical state model implies that at weak ac fields, losses should disappear.[3] Rollins and Silcox[5] claimed that their experiment on Pb-2% In alloy confirmed this prediction. On the other hand, the observed ac response of Nb samples[12] in ac fields with amplitude $h_0 \sim 0.01$ Oe, which was considerably smaller than used in Ref. 5, showed losses already at 10 Hz in SSS. Our measurements on Nb and ZrB_{12} single crystals also showed that the out-of-phase component of the ac susceptibility χ_1'' was finite at low excitation levels[14] and did not have any tendency to vanish. In addition, an experiment demonstrated the low-frequency dispersion of the susceptibility in SSS.[5,14,15] We consider all these results as an indication of the inadequacy of the critical state model for a proper description of the ac response in SSS.

The physical mechanism of the low-frequency losses in the SSS is not clear in spite of a long time (almost 50 years) of efforts. The lack of clear physical picture stimulates further experimental investigations into the low-frequency dy-

namics in other materials. Superconductor YB_6 has some advantages due to its actually ideal type-II magnetization curve.[16] This permits one to avoid additional problems involved in treating the experimental data.

YB_6 is one of the boride family with considerably large $T_c \leq 8.4$ K. The next large $T_c \approx 6.0$ K in this family is found for ZrB_{12}. These two superconductors have different magnetic and surface properties. YB_6 is a classical type-II superconductor[17] ($\kappa \approx 3.0-3.6$), while ZrB_{12} (at least, for temperatures above 4.5 K) is almost type-I ($\kappa \approx 0.75$) superconductor.[14] Near the surface the GL order parameter is enhanced in the ZrB_{12} sample[14] and suppressed in YB_6 (see our tunneling data below).However the ac properties of these materials are similar and we expect that the physical mechanism of the low-frequency response has a universal character.

This paper presents a detailed experimental study of the ac properties of YB_6 single crystal in the SSS. We demonstrated that for $H_0 > H_{c2}$ the dc magnetic moment completely disappeared, while the ac response exhibited the presence of the surface superconductivity. Increasing H_0 above H_{c2} revealed a loss maximum in a field between H_{c2} and H_{c3} with the magnitude considerably larger than in the mixed or normal states. In some dc fields the frequency dependence of the real part of the susceptibility reminds one of the spin-glass systems. At the same time the imaginary component exhibits frequency dispersion which is not a typical feature of the classical spin-glass response. Analysis of the experimental data with the Kramers–Kronig relations (KKRs) showed the possible existence of the loss peak at very low frequencies. We found that the amplitude of the third harmonic was not a cubic function of the ac amplitude (as follows from the perturbation theory) even at very low excitation levels. It was shown that the critical state model could not adequately describe the existing experimental data. A theoretical model based on the slow relaxing order parameter provides qualitative understanding in the origin of partial shielding and losses for $H_0 > H_{c2}$.

II. EXPERIMENTAL DETAILS

A. Sample preparation

The yttrium hexaboride single crystal was grown by the inductive floating zone method under 1.2 MPa of argon by using a powder sintered rod with an optimal composition of $YB_{6.85}$. According to the Y-B phase diagram the composition with the Y:B=1:6 ratio undergoes peritectic melting,[18] and irrespective of this ratio, the YB_4 single crystal with preferential orientation [001] begins to grow. After enrichment of the melting zone by boron (flux modification method) the cubic yttrium hexaboride single crystals with the [100] orientation grow. The composition obtained is $YB_{5.79\pm0.02}$ with a lattice parameter of 4.1001(4) Å which fits well with the published data.[19] The total impurity concentration is less than 0.001% in weight. The obtained single crystals exhibited a sharp superconducting transition at $T_c \approx 7.15$ K.

B. Tunneling measurements

Measurements of the tunneling spectra were carried out using a home-made scanning tunneling microscope (STM). The YB_6 single crystal was mounted inside the cryogenic scanning tunneling microscope and then cooled down to 4.3 K. The dI/dV vs V tunneling spectra were acquired using a conventional lock-in technique while momentarily disconnecting the feedback loop.

C. dc and ac measurements

Magnetization curves were measured using a commercial superconducting quantum interference device (SQUID) magnetometer. In-phase and out-of-phase components of the ac susceptibility at the fundamental frequency and the response at the third harmonic were measured using the pick-up coil method.[5,20] A home-made setup was adapted to the SQUID magnetometer. The block diagram of the experimental setup was published in Ref. 15. The YB_6 crystal ($10 \times 3 \times 1$ mm^3) was inserted into one coil of a balanced pair. The unbalanced signal as a function of the external parameters such as temperature, dc magnetic field, frequency, and amplitude of excitation was measured by a lock-in amplifier. The experiment was carried out as follows. The sample was cooled down in zero magnetic field and then a dc magnetic field was applied. The amplitude and phase of the unbalanced signal were measured. The excitation amplitude was in the range 0.0005–0.5 Oe. We assume that in zero dc field at low temperatures the losses are negligible and the ac in-phase component, χ_1', does not depend on frequency and equals $-1/4\pi$. This assumption permits us to get the values of χ_1' and χ_1'' in absolute units at other dc fields and temperatures. Both H_0 and h_0 fields were parallel to the longest sample axis.

III. EXPERIMENTAL RESULTS

A. Tunneling characteristics

Direct information about the energy-gap value $\Delta_0 \equiv \Delta(T=0)$ at the surface of YB_6 was obtained from the tunneling spectra. The ratio $2\Delta_0/T_c$ is a well-known indicator of the electron-phonon coupling strength.[21] Earlier tunneling studies of YB_6 were performed on a single crystal[17] and on thin films.[22] The obtained values of Δ_0 were 1.22 (Ref. 17) and 1.24 meV,[22] which yields the ratio $2\Delta_0/T_c \approx 4$. In both cases the tunneling took place from underlying layers and revealed strong coupling in the bulk. This ratio was confirmed by Lortz *et al.*[16] who measured the deviation function $D(T) = H_c(T)/H_c(0) - [1-(T/T_c)^2]$ and reported that the $2\Delta_0/T_c$ value is slightly above 4.0. Our tunneling results were obtained by STM and therefore reflect better the density of states at the surface. In contrast to our previous measurements on ZrB_{12} single crystals that exhibited very high spatial homogeneity on the surface,[14] the YB_6 surface has large degraded parts which give rise to featureless tunneling spectra. In other regions, however, the reproducible ratio of the differential conductances in superconducting and normal states $(dI/dV)_s/(dI/dV)_n$ showed clearly BCS-type gap structures (Fig. 1).

The obtained spectra were compared with a temperature-smeared version of the Dynes formula[23] which takes into account the effect of incoherent scattering,

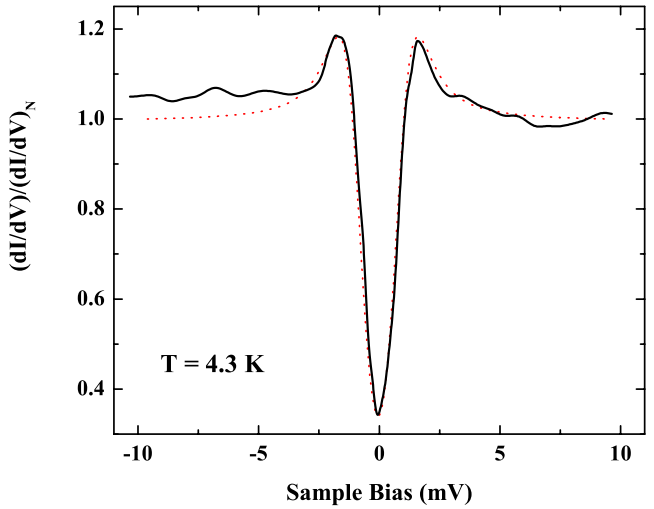

FIG. 1. (Color online) Tunneling spectrum on the surface of YB_6 single crystal at $T=4.3$ K (solid line) and the fit by the Dynes function (dashed line). The fitting parameters are $\Delta(T)=1.0$ meV and $\Gamma=0.10$ meV. The spectrum was normalized to the normal tunneling conductance at 5 meV which is well above the superconducting gap.

$$N_S(E) = N_N(0)\mathrm{Re}[(E - i\Gamma)/\sqrt{(E - i\Gamma)^2 - \Delta^2(T)}]. \quad (1)$$

A good fit to the experimental data at 4.3 K (except for a small unclear difference of the normal resistance at negative and positive biases) was achieved with $\Delta=1.0$ meV and $\Gamma=0.10$ meV. Assuming the BCS $\Delta(T)$ dependence[24] we have obtained the zero-temperature value $\Delta_0=1.1$ meV and $2\Delta_0/T_c \approx 3.59$. This value is very close to the BCS weak-coupling quantity (3.53). In contrast to ZrB_{12} we see that in YB_6 the electron-phonon coupling is suppressed at the surface and corresponds to the weak-coupling limit.[24]

B. dc and ac magnetic characteristics

Figure 2 shows the temperature dependence of the dc magnetic moment at $H_0=10$ Oe. The measurements were

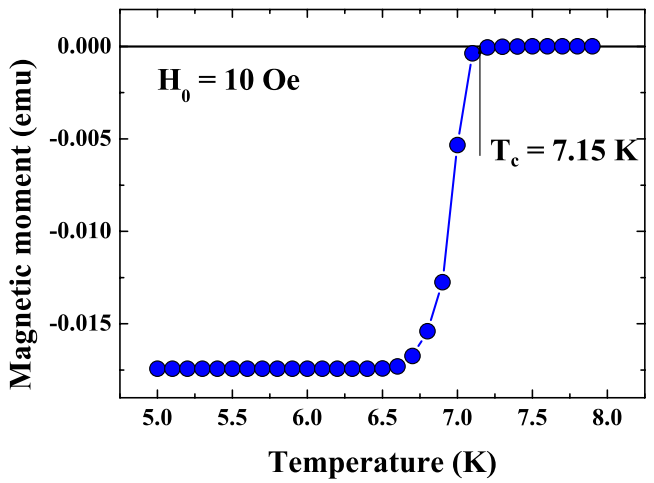

FIG. 2. (Color online) Zero-field cooling (ZFC) temperature dependence of the dc magnetic moment at 10 Oe.

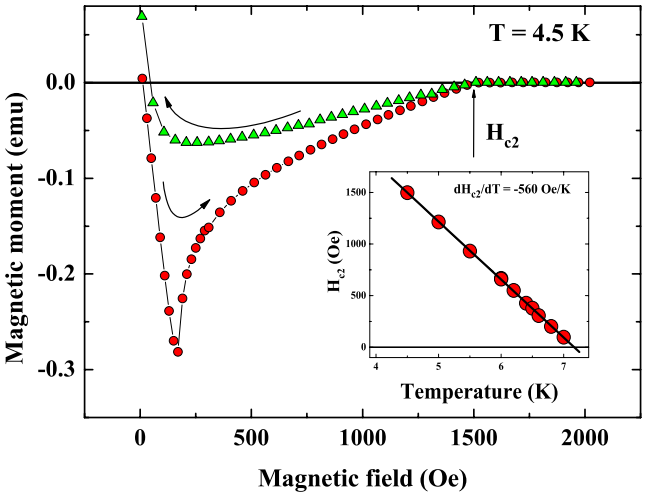

FIG. 3. (Color online) ZFC magnetization curve at $T=4.5$ K. Inset: temperature dependence of H_{c2}.

carried out as follows. The sample was cooled down at zero magnetic field then, after applying a dc magnetic field of 10 Oe, the temperature dependence of magnetic moment was measured. This curve clearly demonstrates that $T_c \approx 7.15$ K. Figure 3 shows the magnetization curve measured at $T=4.5$ K, from which the thermodynamic critical field H_c and the GL parameter κ can be obtained. We consider that the knee on the magnetization curve corresponds to $H_{c2} \approx 1500$ Oe. The specific-heat measurements[16] gave the same value of H_{c2}. Hysteresis near H_{c2} is very small (Fig. 3 and the inset of Fig. 12 of Ref. 16) and we use the known Abrikosov expression for the equilibrium magnetization near $H_{c2}dM/dH_0|_{H_0=H_{c2}}=1/4\pi\beta_A(2\kappa^2-1)$, where $\beta_A=1.18$. It provides GL parameter $\kappa=3.3$. From $\kappa=H_{c2}/\sqrt{2}H_c$ we obtain the thermodynamic critical field $H_c=321$ Oe at 4.5 K. The magnetization loop provides an alternative method of the determination of (Ref. 25), which yields $H_c=295$ Oe. Taking into account that $H_{c2}=1500$ Oe we obtain $\kappa=3.58$. The specific-heat measurements of the same sample gave $H_c=345$ Oe and $\kappa=3.08$.[16] Actually, all these approaches give nearly the same values for the thermodynamic critical field and parameter κ. The London penetration depth at $T=0$ $\lambda_L(0) \approx 1.4\times10^{-5}$ cm was estimated from $1/\lambda_L(0) = \sqrt{\frac{\pi T_c}{\phi_0\kappa_1^2}\left|\frac{dH_{c2}(T_c)}{dT}\right|}$,[26] where $dH_{c2}/dT \approx -560$ Oe/K.

Fourier analysis of the magnetization $M(t)$ in an external field $H(t)=H_0+h_0\cos(\omega t)$ yields $M(t)=M_0(H_0,h_0)+\Sigma_n \frac{1}{2}\chi_n(H_0,h_0)h_0\exp(-in\omega t)$. We show below the results obtained for χ_1 and χ_3 susceptibilities only. The dc field dependencies of χ_1' and χ_1'' at $T=4.5$ K and several frequencies and amplitudes are shown in Figs. 4 and 5. It is seen that curves shift toward higher dc fields when frequency increases (Fig. 4). On the other hand, increasing the ac amplitude shifts the curves toward lower dc fields (Fig. 5). Similar effects were reported for a Pb-2% In sample in Ref. 5. Typical magnetic-field dependence of the third-order nonlinear response $|\chi_3|$ for $h_0=0.05$ Oe and various frequencies is presented in Fig. 6. When the frequency increases, the maximum of χ_3 moves toward higher dc fields, as observed for χ_1'' (Fig. 4).

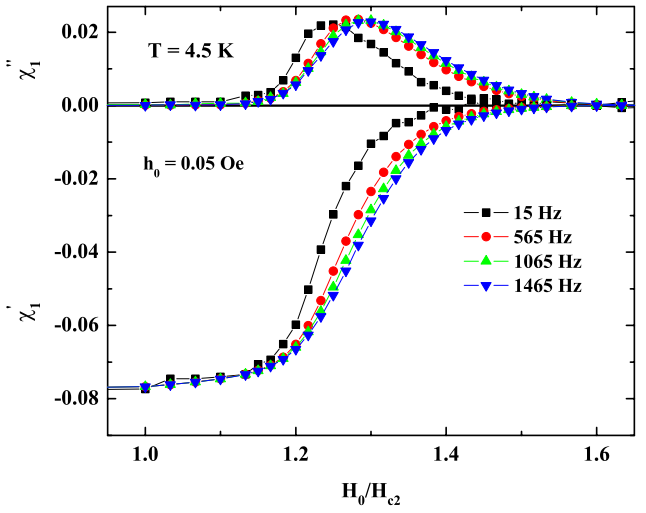

FIG. 4. (Color online) Magnetic-field dependencies of χ_1' and χ_1'' at $T=4.5$ K at different frequencies.

The field dependence of $|\chi_3|$ at 1465 Hz for several amplitudes of excitation h_0 is demonstrated in Fig. 7. Figure 7 shows that for $H_0/H_{c2}=1.3$ $|\chi_3|$ depends strongly on the h_0, while for $H_0/H_{c2}>1.45$ all three curves collapse into one curve. Therefore, the third harmonic susceptibility cannot be described adequately by perturbation theory which predicts $|\chi_3| \propto h_0^2$. Indeed, we find that $|\chi_3| \propto h_0^p$, but the exponent p is not constant and depends on H_0, for example, at $H_0/H_{c2}=1.3$ $|\chi_3| \propto h_0^{0.2}$ and for $H_0/H_{c2}>1.45$ $p=0$.

The observed frequency dispersion of χ_1 and χ_3 for $H_0>H_{c2}$ could be illustrated by a Cole–Cole plot. Figure 8 exhibits the two parametric Cole–Cole plots, namely, χ_1'' [panel (a)] and $|\chi_3|$ [panel (b)] as a function of χ_1' for $H_0>H_{c2}$. Frequency and dc magnetic field are parameters in this plot. Each part of the curves corresponds to some dc field and the arrows show the direction of increase in the frequency. The figure shows that for low fields the increasing of frequency (at a constant dc field) leads to a decrease in both χ_1'' and $|\chi_3|$. On the other hand, for higher fields these quantities increase with the frequency.

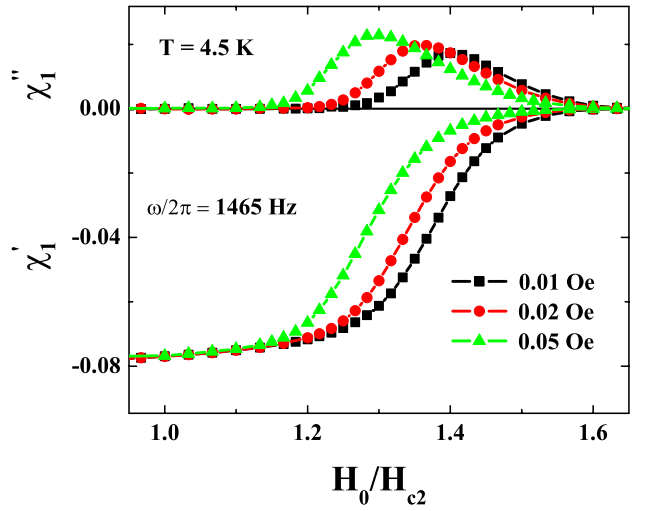

FIG. 5. (Color online) Magnetic-field dependencies of χ_1' and χ_1'' at $T=4.5$ K at various amplitudes.

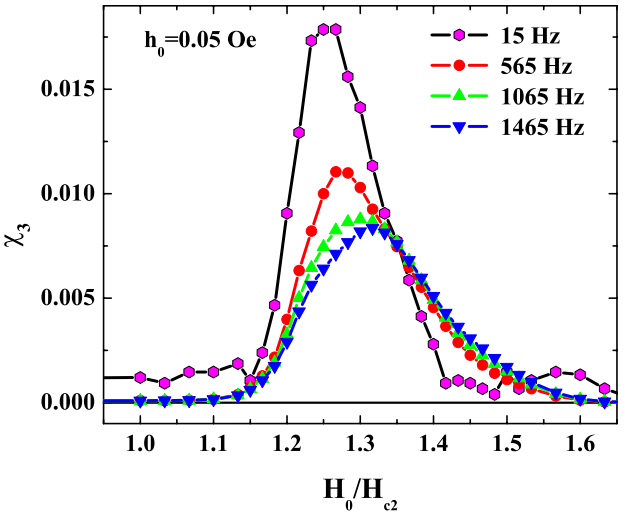

FIG. 6. (Color online) The third-order susceptibility $|\chi_3|$ versus dc magnetic field H_0/H_{c2} at various frequencies.

Figure 9 demonstrates the field dependence of χ_1 at frequency 1065 Hz and $h_0=0.05$ Oe at various temperatures. The peak in χ_1'' shifts toward H_{c2} with the temperature, and at 7 K it locates even *below* H_{c2}. For $T<7$ K we observed the complete shielding ($\chi_1'=-1/4\pi$) in weak dc fields, while only partial shielding was observed at 7 K. The maximum in the third harmonic moves toward H_{c2} with the temperature and at 7 K lies below H_{c2} around $H_0/H_{c2}\approx 0.7$ (Fig. 10). Note that at low temperatures neither the absorption peak nor the third harmonic signal was observed in the mixed state (below H_{c2}). This implies that the SSS is responsible for these effects even at $T=7$ K. This result confirms the coexistence of the SSS and Abrikosov vortices which was proposed by Fink[27] in 1965 but was not clearly observed earlier.

We define H_{c3} as the dc field in which both χ_1' and $|\chi_3|$ become zero. Experiment shows that the H_{c3}/H_{c2} ratio decreases with temperature. In the normal state if $H_0>H_{c3}$ or $T>T_c$ $\chi_1'' \propto \omega$. So, for used in our experiment frequencies the skin depth is considerably larger than the thickness of the

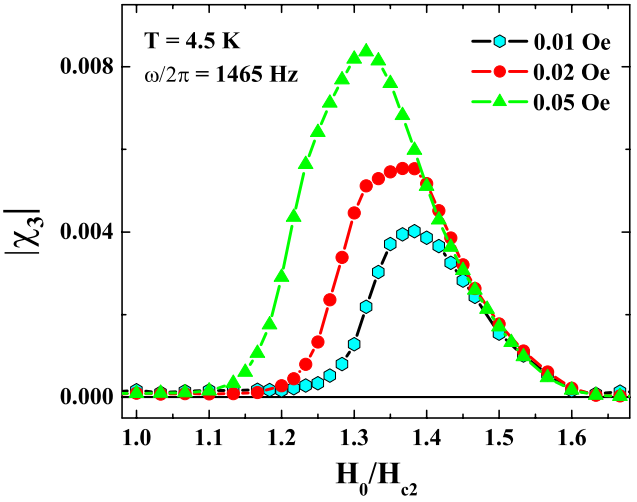

FIG. 7. (Color online) Third-order susceptibility $|\chi_3|$ versus reduced magnetic field H_0/H_{c2} at several amplitudes of excitation.

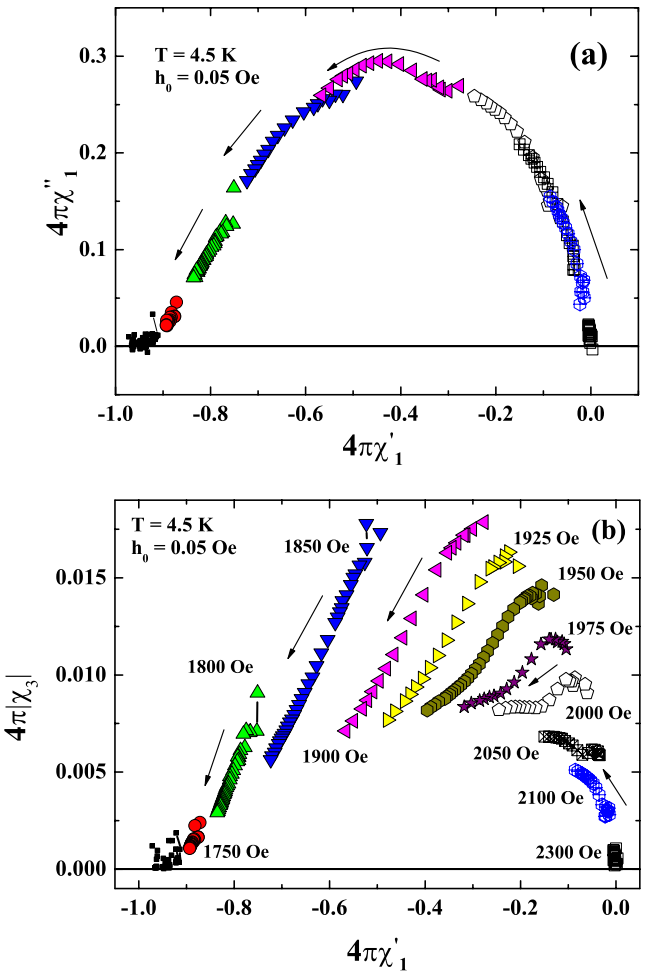

FIG. 8. (Color online) Panel (a): Cole–Cole plot of the χ_1'' as a function of χ_1' for various dc magnetic fields and frequencies. Panel (b): $|\chi_3|$ versus χ_1'. The same symbols on both panels correspond to the same dc field (H_0).

sample and the observed phenomena for $H_{c2}<H_0<H_{c3}$ are caused by the superconducting surface sheath.

IV. THEORETICAL MODEL

We consider the model of infinite superconducting slab of thickness $2L$ in external dc and ac parallel magnetic fields. Due to the considerably short relaxation time of the order parameter[24,28] the stationary GL equations could be used. Looking for the dimensionless order parameter in the form $\Psi(x,y,t)=\phi(x,t)\exp(iky)$, the GL equations could be written as

$$\ln(T_c/T)\{-\phi+|\phi|^2\phi\}-\frac{d^2\phi}{dx^2}+(a-k)^2\phi=0, \qquad (2)$$

$$\frac{d^2a}{dx^2}=\frac{\ln(T_c/T)}{\kappa^2}|\phi|^2(a-k), \qquad (3)$$

where a is the y component of the dimensionless vector potential. The order parameter is normalized with respect to the absolute value at zero dc field. The distances are normalized

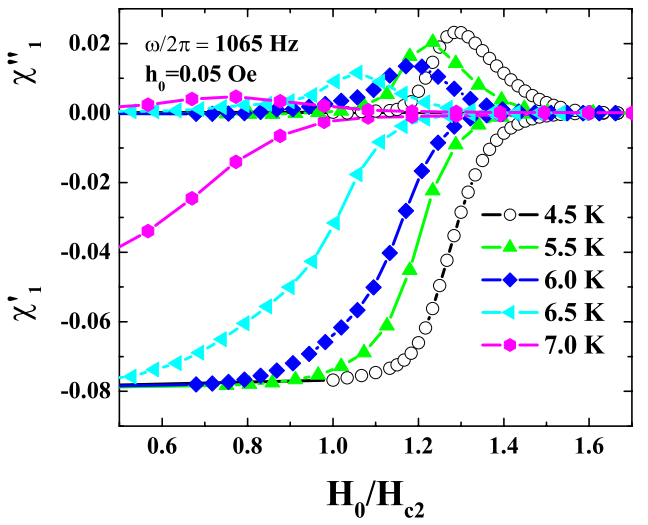

FIG. 9. (Color online) Field dependence of χ_1' and χ_1'' for various temperatures.

with respect to the coherence length at zero temperature ξ_0 ($x\to x/\xi_0$, $y\to y/\xi_0$, $l=L/\xi_0$) and the vector potential is normalized with respect to $\hbar c/2e\xi_0$ [$a=A/(\hbar c/2e\xi_0)$]. For the chosen coordinate system the x axis is perpendicular to the slab surface and the plane $x=0$ is in the center of the slab. The external magnetic fields are along the z axis and the vector potential has only y component. The boundary conditions which define the surface states are $\phi(0,t)=0$, $a(0,t)=0$ and $d\phi(l,t)/dx=0$, $da(l,t)/dx=\mathfrak{h}(t)$, where $\mathfrak{h}(t)$ is the dimensionless applied magnetic field. We took into account that the magnetic field at both sides of the slab had the same values and we could consider only the half space $x>0$. These nonlinear equations could be solved by numerical methods. We add the time derivative $\partial\phi/\partial t$ to the right side of Eq. (2) and look for the stationary solutions of Eqs. (2) and (3). Replacing the space derivatives by finite differences on the grid with step $dx=l/N$, Eq. (2) is transformed to N first-order differential equations. The stationary solution of

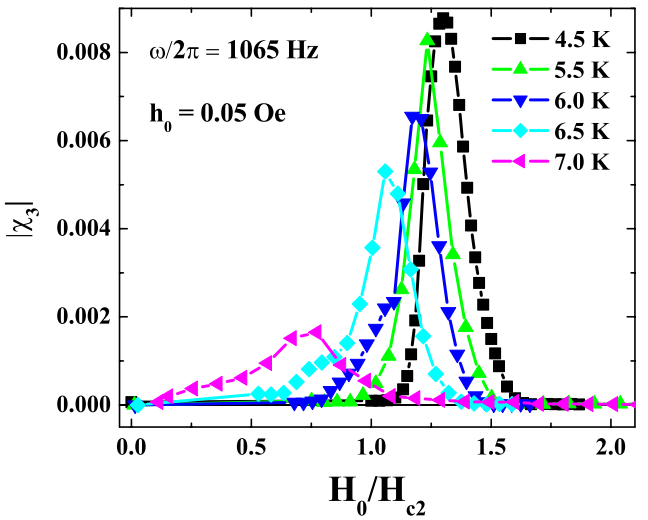

FIG. 10. (Color online) Field dependence of $|\chi_3|$ for some temperatures.

these equations can be found by regular methods. A grid with $N=1000$ points was used. In the SSS the order parameter differs from zero only near the surface at a scale of several coherence lengths $\xi(T)$. Actually, the choice $L=5\xi(T)\equiv D$ provides good accuracy for the calculation of ϕ. The parameter k is not a gauge-invariant quantity and we fix the gauge by the condition $a=0$ at $x=0$. Note that the real sample dimensions exceed $\xi(T)$ by 3–5 orders of magnitude. In the SSS the magnetic field in the bulk is constant. Therefore the vector potential in the surface layer for a thick slab can be expressed via the solution for a thin slab with thickness D as

$$a(l-d+x)=a_s(x)+\mathfrak{h}_{zs}(l-d), \tag{4}$$

where $d\equiv D/\xi_0$. The gauge-invariant quantity is the superconducting velocity $V\propto(a-k)$ and the corresponding transformation of k is

$$k=k_s+\mathfrak{h}_{zs}(l-d). \tag{5}$$

The index s corresponds to the problem for a thin slab and $\mathfrak{h}_{zs}$ is the z component of the magnetic field in the center of the thin slab. This note is important for numerical calculations.

It is well known (see, for example, Ref. 15) that for a given external magnetic field there is a whole band of k for which surface solutions exist, and these solutions describe in general the nonequilibrium states. Only one k corresponds to the equilibrium state for which the magnetic field inside the bulk equals the external one and the total surface current J_s is zero. This parameter for a finite sample is analogous to the number of giant vortices.[11] The k is an integral constant of the nonstationary GL equations. On the other hand, the relaxation time in the GL equations is considerably shorter than any period of ac field in our experiment. Thus, we could expect that during an ac cycle ϕ follows the instantaneous value of the magnetic field while k remains approximately constant. Let us assume that we start from an equilibrium state in some dc field H_0 and then we increase H_0 while simultaneously keep k constant. Then J_s does not equal to zero now and we could define the surface critical current as $J_c=c/4\pi(H_1-H_0)$, where H_1 is the field at which the SSS energy becomes equal to the normal-state energy.[13,29] Actually $dH_{s1}\equiv H_1-H_0$ depends on the sample thickness, as it is shown in Fig. 11, due to large magnetic energy which arises when the field inside the bulk differs from the external field. The assumption of slow relaxing k enables us to understand qualitatively the complete screening of a weak ac field with amplitude $h_0\ll H_0$ in SSS. The ac surface current $J_s[k,H(t)]$ is a function of the instant value of external magnetic field $H(t)=H_0+h_0\cos(\omega t)$ and k. This function could be expressed through $J_s(k_s,H)$, the solution for the thin slab, i.e., with thickness $L=5\xi(T)$. For a thick slab we could express k_s through k using Eq. (5). Direct calculation shows that the magnetic field in the center of the thin slab h_{c0} as a function of H and constant k_s actually equals the external field, i.e., surface current $J_s(k_s,H)$ is small and the complete penetration takes place. For example, at $T=0.9T_c$ $\frac{\partial h_{c0}(k_{s,\mathrm{eq}},H)}{\partial H}=0.88+0.19(H/H_{c2}-1)\simeq 1$. Here $k_{s,\mathrm{eq}}$ is the equilibrium value of k_s in given H. For a thick slab with $L\gg 5\xi(T)$ and $k\neq k_s$ the condition of constant k during the ac cycle implicitly means that k_s also changes according to Eq. (5). This leads to considerably large surface currents and to the shielding of the ac field. Actually we have another large dimensionless parameter $L/\xi(T)$ that increases the screening in the thick slab. Figure 12 demonstrates the calculated (in the assumption of constant k) $\chi'=\partial M/\partial H$ as a function of the dc field. It is evident that for any macroscopically large sample the complete screening $\chi'=-1/4\pi$ should be observed at all dc fields, excluding fields immediately close to H_{c3}. The experiment (Fig. 4) does not confirm this conclusion. It was observed that at a field, i.e., $H_0/H_{c3}\approx 1.3$, $|\chi_1'|<1/4\pi$. It means that k is a not constant parameter and its slow relaxation (in comparison with GL relaxation rate) results in losses and incomplete shielding.

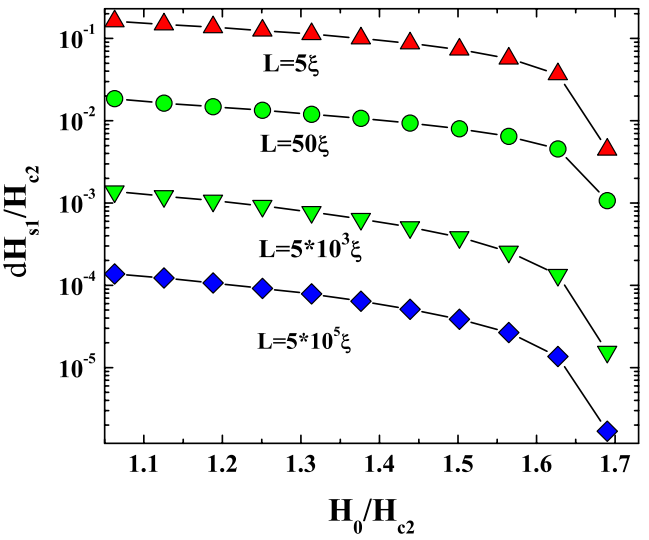

FIG. 11. (Color online) Field dependence of the surface critical magnetic field—$dH_{s1}(H_0/H_{c2})$ for different slab thicknesses L at $T/T_c=0.9$. Here $dH_{s1}\equiv H_1-H_0$ (see text).

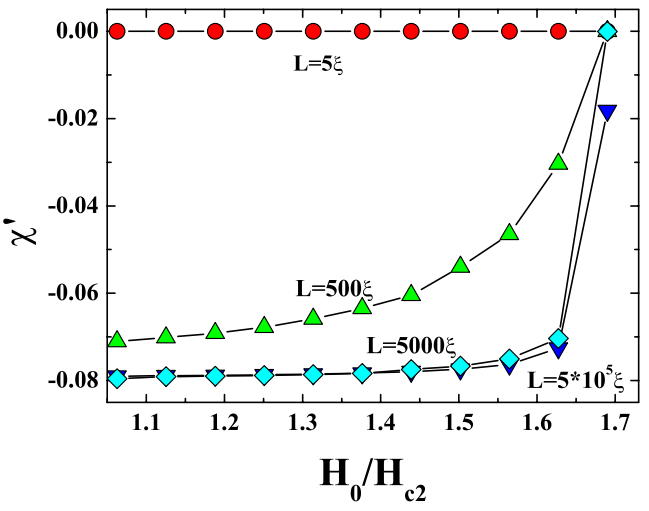

FIG. 12. (Color online) Field dependence of χ_1' for different slab thicknesses L at $T/T_c=0.9$. It is assumed that during ac period the parameter k is kept constant.

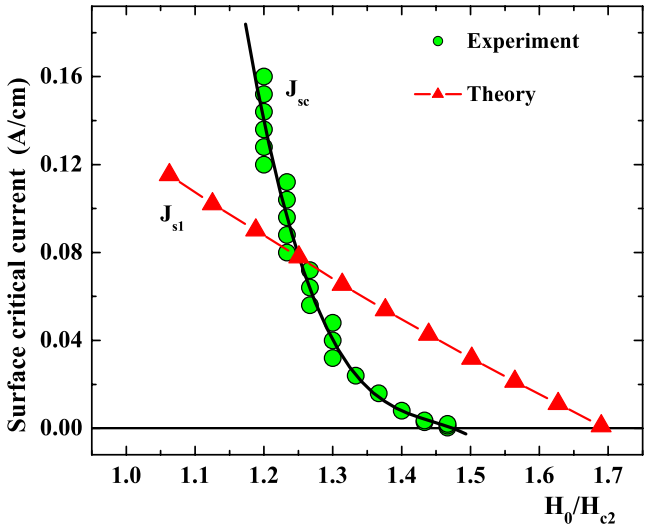

FIG. 13. (Color online) Experimental and theoretical values of surface critical current as a function of reduced dc field H_0/H_{c2}. Experimental data were obtained with the approach proposed in Ref. 30 (see text).

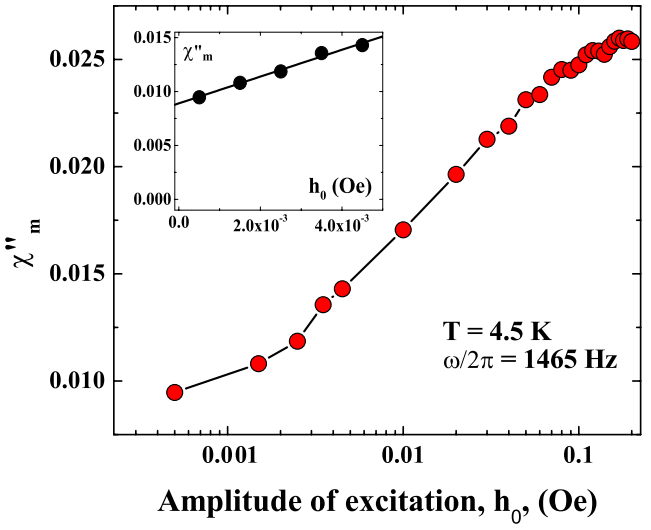

FIG. 14. (Color online) Out-of-phase susceptibility at maximum χ_m'' as a function of an excitation amplitude h_0. The inset shows the expanded view for low h_0 in a linear scale.

V. DISCUSSION

A. Critical currents and losses

For a given ac amplitude χ_1'' has a maximum at some dc magnetic field H_m (see Fig. 5). $H_m(h_0)$ was considered in Ref. 30 as the dc field at which the amplitude of the ac surface current $J_{sc}=(c/4\pi)h_0$ is approximately equal to the critical value $J_c(H_0)$. In order to test this assumption we show in Fig. 13 the experimental $J_{sc}(H_0)$ and calculated $J_c(H_0)$ for a slab of thickness $L=5\times10^5\xi$. The theoretical plot was normalized in order to obtain the intersection with the experimental curve at $H_0/H_{c2}=1.25$. While $J_c(H_0)$ is almost linear and $J_c(H_{c3})=0$, the experimental curve is nonlinear and starts from $H_0/H_{c2}=1.45$. Therefore, we conclude that the proposed method of experimental determination J_{sc},[30] which was used in a number of publications, needs more detail consideration.

In Fig. 14 we present the maximum $\chi_1''(H_m)$ values as a function of h_0 (see also Fig. 5). The inset shows the extended plot at low amplitudes in a linear scale and it is seen that in the limit $h_0\to0$ losses still exist. For a linear system χ_1'' should be amplitude independent while our experiments show an amplitude dependence of $\chi_m''(h_0)$ at low excitation levels. This indicates that the ac response is not linear one, even at very low excitation amplitudes. More experimental measurements in low ac fields are needed to clarify these observations.

B. Kramers-Kronig analysis

Application of the KKRs permits us to reveal the existence of the large absorption peak at very low frequencies. In general, the magnetic moment of the sample could be presented as

$$M(t)=\int_{-\infty}^{t}K[t-t',h(t')]h(t')dt'. \tag{6}$$

For low amplitude $h_0\simeq0.02$ Oe the susceptibilities at higher harmonics are small and Eq. (6) could be rewritten as

$$M(t)=\int_{-\infty}^{t}K(t-t',h_0)h(t')dt'. \tag{7}$$

In this approximation the response at the fundamental frequency matches the KKR,

$$\chi_1'=\chi_\infty+\int_0^\infty\frac{2\zeta\chi_1''(\zeta)}{\pi(\zeta^2-\omega^2)}d\zeta. \tag{8}$$

We can rewrite Eq. (8) as

$$\begin{aligned}I(\omega)\equiv\chi_1'(\omega)-\int_{\omega_0}^{\omega_m}\frac{2\zeta\chi_1''(\zeta)}{\pi(\zeta^2-\omega^2)}d\zeta\\=\chi_1''(\varpi)\int_0^{\omega_0}\frac{2\zeta d\zeta}{\pi(\zeta^2-\omega^2)}+\chi_\infty\\+\sum_n\int_{\omega_m}^\infty\frac{2\omega^{2n}\chi_1''(\zeta)}{\pi\zeta^{2n+1}}d\zeta,\end{aligned} \tag{9}$$

where ω_0 and ω_m are the minimal and maximal available frequencies in our experiment, respectively, and $0<\varpi<\omega_0$. The quantity $I(\omega)$ can be calculated directly from the available experimental data and be fitted as

$$I(\omega)=a+b\ln|1-\omega_0^2/\omega^2|+\sum_{n=1}^{n_{\max}}c_n\omega^{2n}, \tag{10}$$

where $c_n>0$ and $\chi_1''(\varpi)=\pi b$. For $\omega^2/\omega_m^2\ll1$ it is sufficient to take into account only a few terms in Eq. (10). Results of this procedure are presented in Fig. 15 where $\chi_1''(\varpi)$ and a are shown as a function of the dc field. Experimental data in

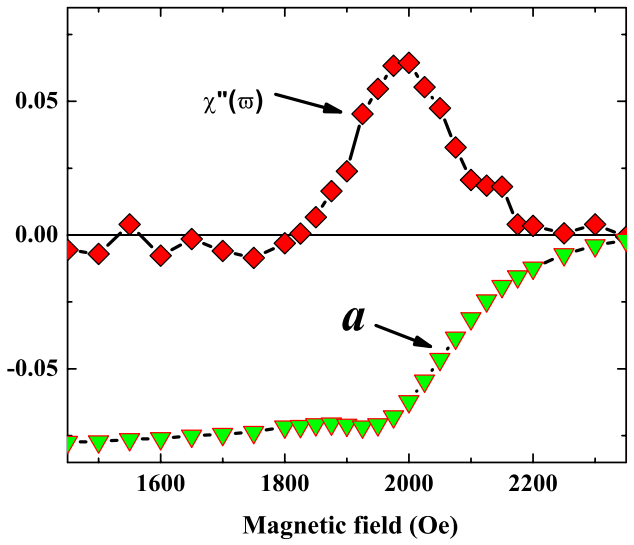

FIG. 15. (Color online) Field dependencies of $\chi''(\varpi)$ and parameter a of Eq. (10) at $T=4.5$ K and $h_0=0.02$ Oe (see text).

the frequency range 15–1460 Hz and $T=4.5$ K were used for the calculation of $I(\omega)$ for $25<\omega/2\pi<200$ Hz with $\omega_0/2\pi=17.5$ Hz and $\omega_m/2\pi=1455$ Hz. The fit of $I(\omega)$ in Eq. (10) with $n_{\max}=1$ provides the curve $\chi_1''(\varpi)$, shown in Fig. 15. Estimation of $c_n \approx \omega^2 c_{n-1}/\omega_m$ with $\omega^2/\omega_m^2 \approx 0.02$ allows us to use only one term in the sum in Eq. (10) to provide the correct result. Figure 15 shows that the calculated loss peak is approximately three times larger than that shown in Fig. 4. The evidence that outside the frequency region (ω_0, ω_m) there are considerable losses could be obtained from a direct calculation of the integral on the left side of Eq. (9), $R=\int_{\omega_0}^{\omega_m} \frac{2\zeta\chi_1''(\zeta)}{\pi(\zeta^2-\omega^2)} d\zeta$. Figure 16 shows the frequency dependence of R for $H_0=2000$ Oe.

Note that R is positive for $\omega/2\pi<1000$ Hz which means that the left side of Eq. (9) is the sum of the two negative values. So one should expect a large contribution to the integral in Eq. (8) from frequencies outside the (ω_0, ω_m) interval. Direct calculation yields a large b in Eq. (10).

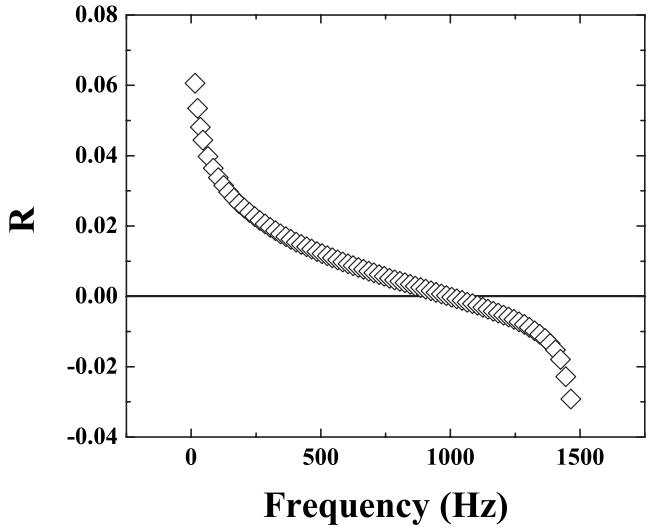

FIG. 16. Frequency dependence of the parameter R.

C. Surface vortices

We consider that the observed losses in SSS are the result of the slow relaxation of k to its equilibrium value. This model can describe the partial screening and the losses for $H_0>H_{c2}$. The alternative model supposes that the ac response for $H_0>H_{c2}$ is formed by two-dimensional (2D) surface vortices.[31,32] These vortices with a surface density $n_s=H_0 \sin(\theta)/\phi_0$ appear if the applied field has a normal component to the sample surface due to misalignment or the surface is not sufficiently smooth. Here θ is the angle between the direction of the magnetic field and the sample surface. To the best of our knowledge, the conductivity of the surface vortex layer has not yet been calculated. Therefore we use the analog of the Bardeen-Stephen expression for Abrikosov vortices,

$$\sigma = \sigma_n H_{c2}/H_0 \sin(\theta), \tag{11}$$

where σ_n is the conductivity in the normal state. Our measurements show that at 4.5 K $\sigma_n \approx 0.8\times 10^{17}$ cgs and this value is in good agreement with data provided in Ref. 16. The skin depth, corresponding to this conductivity, at 10 Hz for any real misalignment $\simeq 10^{-2}$ rad is approximately 5 cm. This value is much larger than the layer with thickness order of ξ, 10^{-6} cm, to provide any shielding. To obtain the observed shielding we have to assume that the correct estimation of the surface layer conductivity exceeds the given by Eq. (11) value about 8 orders of magnitudes.[33] In the tilted dc field, when the surface vortex density increases, losses do not exhibit any considerable increasing.[34] We consider that surface vortices do not play the essential role in our experiments.

D. Glasslike behavior

The ac response of SSS resembles the response of a spin-glass system. The real and the imaginary parts of χ_1 can be well represented by a low-order polynomial of $\ln(\omega)$ as shown in Fig. 17 for $H_0=2$ kOe and $T=4.5$ K.

In this figure χ_1' and χ_1'' are presented by

$$a_0 + a_1 \ln(\omega) + a_2 \ln^2(\omega) \tag{12}$$

for a wide frequency range 15–1465 Hz. At some dc fields a_2 in Eq. (12) is small and we obtain a spin-glass-like frequency dependence $\chi_1' \propto \ln(\omega)$.

The observed frequency dispersion in a spin-glass systems is due to the presence of a wide spectrum of relaxation times. In analogy with spin-glass system and in accordance with Ref. 12 we could assume that the surface of the sample in the SSS is consisted of supeconducting clusters. The size of these clusters is defined by a characteristic length of surface inhomogeneity. Each cluster has unique dynamical properties. However, this analogy with spin-glass systems is not complete because χ_1'' exhibits frequency dispersion, which is not typical for spin-glass systems, and the "$\pi/2$" rule, $\chi_1''=-\frac{\pi}{2}\frac{d\chi_1'(\omega)}{d\ln(\omega)}$ (Ref. 35), is not fulfilled for our data (Fig. 18).

Let us assume that the magnetic moment $M(t)$ of the cluster could be obtained from the relaxation equation

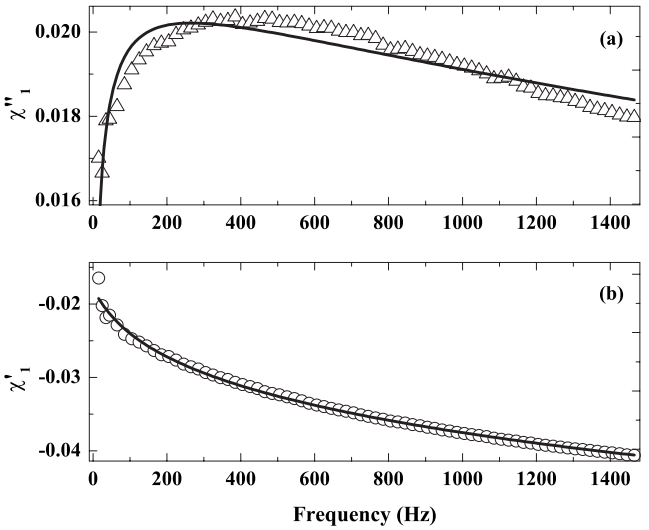

FIG. 17. Frequency dependence of $\chi_1''(\omega)$ [panel (a)] and $\chi_1'(\omega)$ [panel (b)] for $H_0=2$ kOe ($H_0=1.25H_{c2}$) at 4.5 K. Continuous lines present the fit to the second-order polynomial of $\ln(\omega)$ [Eq. (11)].

$$dM/dt = -\nu M - dh/dt. \tag{13}$$

Here the external force is the time derivative dh/dt because in the dc magnetic-field magnetic moment equals zero in SSS. Assuming that the average over all clusters provides the observed ac response, we obtain

$$\chi_1 = \int_0^\infty \tilde{P}(\nu)\frac{i\omega}{\nu - i\omega}d\nu, \tag{14}$$

where $\tilde{P}(\nu)$ is the distribution function of the relaxation rates. Using $1/(\nu - i\omega) = \int_0^\infty \exp[-(\nu - i\omega)t]dt$ we could transform Eq. (14) to

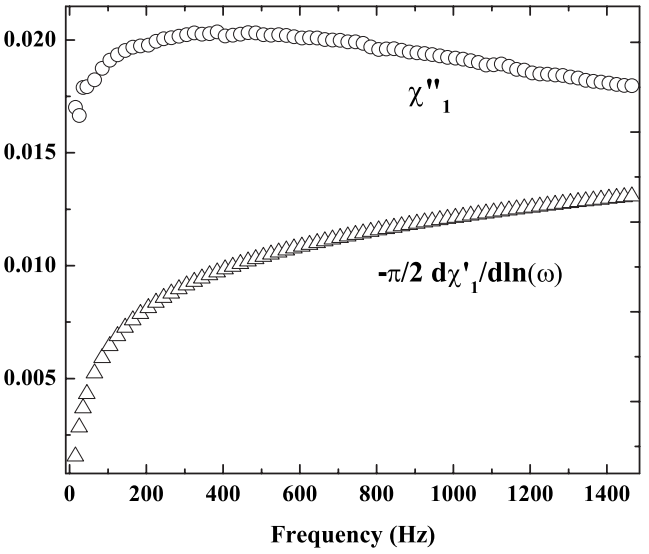

FIG. 18. The test of the "$\pi/2$" rule for the experimental data at $T=4.5$ K and $H_0=2$ kOe.

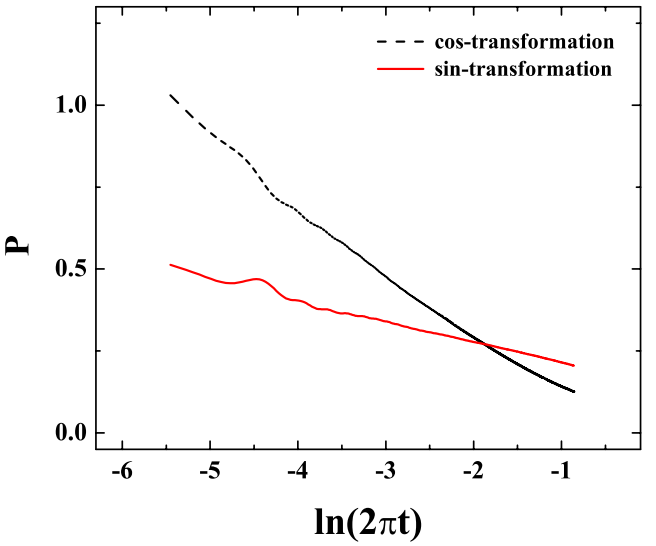

FIG. 19. (Color online) The test of Eq. (16) on the experimental data at $T=4.5$ K and $H_0=2$ kOe.

$$i\chi_1(\omega)/\omega = \int_0^\infty P(\nu)\exp(-\nu t)d\nu, \tag{15}$$

where $P(t)=\int_0^\infty \tilde{P}(\nu)\exp(-\nu t)d\nu$. So, if Eqs. (13) and (14) could adequately describe the experimental data with some $P(\nu)$, then the following expression should be valid:

$$P(t) = 2\int_0^\infty \chi_1''(\omega)\cos(\omega t)d\omega/\pi\omega$$

$$= -2\int_0^\infty \chi_1'(\omega)\sin(\omega t)d\omega/\pi\omega. \tag{16}$$

Experimental data are available only for a finite frequency range 15–1465 Hz, while the integrals in Eq. (16) are expanded for all frequencies, and we have to extrapolate our data to the entire frequency axis. This was done by assuming that at frequencies smaller than 15 Hz and larger than 1465 Hz, χ_1'' is a power function of the frequency. It was found that sine- and cosine-Fourier transformations of Eq. (16) yield different values for $P(t)$, as shown in Fig. 19, where the ac response data in $H_0=1.25H_{c2}$ were used. So, the presented experimental data do not permit to consider the SSS as a spin-glass system.

VI. CONCLUSIONS

We have studied the low-frequency ac response of a YB_6 single crystal, type-II, single-band, and isotropic superconductor. Critical magnetic fields and the GL parameter κ were defined using magnetization curves. Tunneling spectrum measurements showed that in this material the electron-phonon interaction is suppressed near the surface and the BCS weak-coupling limit is realized. ac measurements revealed losses at the fundamental frequency at a very low excitation level in the SSS. The third-order susceptibility exhibits a slow power dependence. These experimental obser-

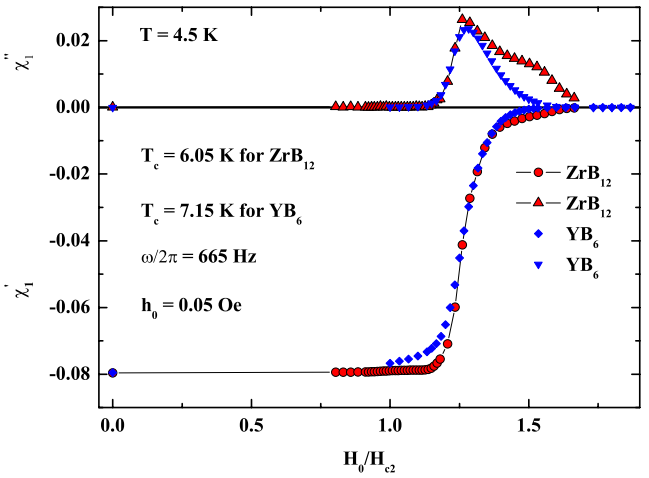

FIG. 20. (Color online) Magnetic-field dependencies of χ_1' and χ_1'' at $T=4.5$ K at ZrB_{12} and YB_6 samples.

vations cannot be described either the critical state model[5,13] or the 2D surface vortices.[31] A model of the slow relaxing order parameter is proposed. This model enables us to understand qualitatively the incomplete shielding and losses at low frequencies in the SSS. The frequency dispersion of χ_1 is well described in terms of $\ln(\omega)$, and for some dc fields $\chi_1' \propto \ln(\omega)$, as for a spin-glass system. However, χ_1'' also shows frequency dispersion that excludes the possibility of a pure spin-glass behavior. Analysis of the experimental data with Kramers–Kronig relations revealed the presence of the loss peak at ultralow frequencies. Coexistence of the SSS and three-dimensional (3D)-Abrikosov vortices was observed near T_c.

The comparison of two superconductors from the boride family, ZrB_{12} and YB_6, shows that they have very distinct magnetic and tunneling characteristics while the ac response is similar. Figure 20 presents field dependence of χ_1' and χ_1'' of ZrB_{12} and YB_6 samples. We see that in reduced dc field H_0/H_{c2} the maximum of χ_1'' is in the same place and actually has equal value. This points out the universality of relaxation processes in the SSS. The line shape of $\chi_1''(H_0)$ curve for ZrB_{12} is more complicated than for YB_6. Analysis of the line shape may be done when the loss mechanisms in the SSS will be clarified. Additional experimental and theoretical studies have to be done in this direction. Detailed comparison of the ac properties ZrB_{12} and YB_6 will be reported in our forthcoming publications.

ACKNOWLEDGMENTS

This work was supported by the Israeli Ministry of Science (Israel–Ukraine fund) and by the Klatchky Foundation for superconductivity. We wish to thank I. Ya. Korenblit and E. B. Sonin for many valuable discussions.

[1] D. Saint-James and P. G. de Gennes, Phys. Lett. **7**, 306 (1963).
[2] M. Strongin, A. Paskin, D. G. Schweitzer, O. F. Kammerer, and P. P. Craig, Phys. Rev. Lett. **12**, 442 (1964).
[3] A. Paskin, M. Strongin, P. P. Craig, and D. G. Schweitzer, Phys. Rev. **137**, A1816 (1965).
[4] J. P. Burger, G. Deutscher, E. Guyon, and A. Martinet, Phys. Rev. **137**, A853 (1965).
[5] R. W. Rollins and J. Silcox, Phys. Rev. **155**, 404 (1967).
[6] H. R. Hart, Jr. and P. S. Swartz, Phys. Rev. **156**, 403 (1967).
[7] A. K. Geim, S. V. Dubonos, J. G. S. Lok, M. Henin, and J. C. Maan, Nature (London) **396**, 144 (1998).
[8] G. M. Braverman, S. A. Gredeskul, and Y. Avishai, Phys. Rev. B **57**, 13899 (1998).
[9] G. F. Zharkov, V. G. Zharkov, and A. Yu. Zvetkov, Phys. Rev. B **61**, 12293 (2000); G. F. Zharkov, Phys. Usp. **47**, 944 (2004).
[10] K. Tanaka, I. Robel, and B. Janko, Proc. Natl. Acad. Sci. U.S.A. **99**, 5233 (2002).
[11] H. J. Fink and A. G. Presson, Phys. Rev. **151**, 219 (1966); **168**, 399 (1968).
[12] J. Kötzler, L. von Sawilski, and S. Casalbuoni, Phys. Rev. Lett. **92**, 067005 (2004).
[13] H. J. Fink and L. J. Barnes, Phys. Rev. Lett. **15**, 792 (1965); H. J. Fink, *ibid.* **16**, 447 (1966).
[14] M. I. Tsindlekht, G. I. Leviev, V. M. Genkin, I. Felner, Yu. B. Paderno, and V. B. Filippov, Phys. Rev. B **73**, 104507 (2006).
[15] G. I. Leviev, V. M. Genkin, M. I. Tsindlekht, I. Felner, Yu. B. Paderno, and V. B. Filippov, Phys. Rev. B **71**, 064506 (2005).
[16] R. Lortz, Y. Wang, U. Tutsch, S. Abe, C. Meingast, P. Popovich, W. Knafo, N. Shitsevalova, Yu. B. Paderno, and A. Junod, Phys. Rev. B **73**, 024512 (2006).
[17] S. Kunii, T. Kasuya, K. Kadowaki, M. Date, and S. B. Woods, Solid State Commun. **52**, 659 (1984).
[18] T. B. Massalski, *Binary Alloy Phase Diagrams Materials* (ASM International, Materials Park, OH, 1990).
[19] *Compounds with Boron, System Number 39*, Gmelin Handbook of Inorganic Chemistry. Sc, Y, La-Lu Rare Earth Elements Vol. C11a, edited by H. Bergman *et al.* (Springer-Verlag, Berlin, 1990).
[20] D. Shoenberg, *Magnetic Oscillations in Metals* (Cambridge University Press, Cambridge, 1984).
[21] J. P. Carbotte, Rev. Mod. Phys. **62**, 1027 (1990).
[22] R. Schneider, J. Geerk, and H. Rietschel, Europhys. Lett. **4**, 845 (1987).
[23] R. C. Dynes, V. Narayanamurti, and J. P. Garno, Phys. Rev. Lett. **41**, 1509 (1978).
[24] M. Tinkham, *Introduction to Superconductivity*, 2nd ed. (Dover, New York, 2004).
[25] D. K. Finnemore, J. E. Ostenson, S. L. Budko, G. Lapertot, and P. C. Canfield, Phys. Rev. Lett. **86**, 2420 (2001).
[26] A. A. Abrikosov, *Fundamentals of the Theory of Metals* (North-Holland, Amsterdam, 1988).
[27] H. Fink, Phys. Rev. Lett. **14**, 853 (1965).
[28] G. I. Leviev, A. V. Rylykov, and M. R. Trunin, Pis'ma Zh. Eksp. Teor. Fiz. **50**, 78 (1989); [JETP Lett. **50**, 88 (1989)].

[29] J. G. Park, Phys. Rev. Lett. **15**, 352 (1965).
[30] B. Bertman and M. Strongin, Phys. Rev. **147**, 268 (1966).
[31] S. Sh. Akhmedov, V. R. Karasik, and A. I. Rusinov, Zh. Eksp. Teor. Fiz. **56**, 444 (1969); [Sov. Phys. JETP **29**, 243 (1969)].
[32] I. O. Kulik, Zh. Eksp. Teor. Fiz. **52**, 1632 (1967); [Sov. Phys. JETP **25**, 1085 (1967)].
[33] C. Kittel, S. Fahy, and S. G. Louie, Phys. Rev. B **37**, 642 (1988).
[34] M. I. Tsindlekht, V. M. Genkin, G. I. Leviev, I. Felner, and N. Yu. Shitsevalova, (unpublished).
[35] E. Pytte and Y. Imry, Phys. Rev. B **35**, 1465 (1987).